



Identifying 8 mm Radio Brightenings During the Solar Activity Minimum

Juha Kallunki¹ · Merja Tornikoski¹ · Irene Björklund¹

Received: 6 March 2020 / Accepted: 18 July 2020 / Published online: 29 July 2020
© The Author(s) 2020

Abstract Strong solar radio brightenings have been extensively studied in the past, and their correlation to the sunspots and active regions are already well known. But even when the Sun is ostensibly quiet, there is practically always some activity that can be detected in the radio domain. In this article we investigate these semi-active features at 8 mm using the radio telescope at Aalto University Metsähovi Radio Observatory. The observations were made between May and September 2019 when the solar activity was very low, and for our detailed study we chose dates when no active regions were identified on the solar surface by the National Oceanic and Atmospheric Administration. The brightness temperature of these radio regions during this quiescent period of solar activity is at maximum approximately 250 K above the quiet-Sun level. We compared our millimeter data with data taken in extreme ultraviolet, and we found that these weak radio brightenings are mostly related to coronal hole features and magnetic bright points. We also found that there are two different categories of bright points: those with and without flux tube structure. The formation of the weak radio brightenings is comparable to the stronger radio brightenings: the rising fluxes from the weak photospheric features can be detected as a radio source.

Keywords Chromosphere, quiet · Solar cycle, observations

1. Introduction

Even when the Sun is ostensibly quiet and there are no visible, classified active regions (ARs) on the solar disk, there is often some activity, such as coronal holes and magnetic bright points. Also solar radio observations practically always detect some activity. During

✉ J. Kallunki
juha.kallunki@aalto.fi

M. Tornikoski
merja.tornikoski@aalto.fi

I. Björklund
irene.bjorklund@aalto.fi

¹ Aalto University Metsähovi Radio Observatory, Metsähovintie 114, 02540 Kylmälä, Finland

the solar activity minimum it is possible to study properties of these weak solar radio features because they can be detected and followed better than during the times when there is ongoing activity in many different locations and intensity scales. In this work we study the connection between weak solar radio brightenings at 8 mm and solar atmospheric features. Observations are made during the solar minimum between Solar cycles 24 and 25, in the Summer season 2019.

Over the past few years we have studied the connection between strong radio brightenings at 8 mm and active regions (sunspots) in various ways (e.g. Kallunki et al., 2012, 2018; Kallunki and Uunila, 2017). The radio brightenings follow the traditional sunspot butterfly diagram quite accurately, excluding high latitudes at the beginning of the solar cycle.

Smirnova et al. (2015) have proposed a scenario for radio source formation at millimetre wavelengths, according to which radio sources are originally connected to a sunspot by rising magnetic fluxes coming from the spot umbra and are formed due to thermalization of accelerated particles. These rising magnetic fluxes are observed as a radio source. The magnetic fluxes do not rise fully vertically upwards, and radio sources and visible sunspots or active regions (ARs) are not observed exactly at the same locations.

Coronal holes are areas of lower density than the quiet-Sun region (Dosc hek et al., 1997) and they are the sources of the fast solar wind. In earlier studies, polar brightenings at millimetre wavelengths have been observed and analysed by Pohjolainen, Rie hokainen, and Valtaoja (1999), Pohjolainen (2000), Rie hokainen et al. (2001), Selhorst et al. (2011), Nitta et al. (2014), Oliveira e Silva et al. (2016), Selhorst et al. (2017), Alissandrakis et al. (2017), Sudar et al. (2019), Rodger et al. (2019). Results have shown that these polar brightenings are associated with holes or coronal bright points. These radio bright areas are also called enhanced temperature region (ETR).

The connection between X-ray bright points and radio sources at centimetre wavelengths was studied by, e.g., Benz et al. (1997). These authors found that these features are correlated, with the correlation between X-rays and radio intensity sources being best at shorter radio wavelengths (1.3 cm).

Solar pores are usually classified as small premature sunspots or sunspot-like features that are characterized by the absence of a penumbra. They are smaller than the traditional sunspots. However, their magnetic field strength on the photospheric level can vary between 600 G to 1700 G, which approximately corresponds to the sunspot magnetic field strength (Sütterlin, Schröter, and Muglach, 1996; Giordano et al., 2008; Cho et al., 2015). Solar faculae are similar bright and small atmospheric features. A strong magnetic field above the active region is often a sign of gyroresonance emission (Bogod, Stupishin, and Yasnov, 2012). The lack of magnetic field usually indicates purely thermal emission. Also, Rodger et al. (2019) have reported that a primary emission mechanism in the quiet chromosphere is actually a thermal emission.

In the following sections we present our instrumentation and observations, method for identifying sources of weak radio brightenings, and the final results.

2. Instrumentation

The RT-14 at Aalto University Metsähovi Radio Observatory (MRO), Finland (Helsinki region; E 24:23.35, N 60:13.04) is a radome-enclosed Cassegrain-type antenna with a diameter of 13.7 m. The usable wavelength range of the telescope is 13.0 cm–2.0 mm. During solar observations the antenna is used for solar mapping, partial solar mapping, and tracking of any selected areas on the solar disk. In this article we focus on data taken at 8 mm.

The beam size of the telescope is 2.4 arc min at 8 mm. The receiver is a Dicke-type radiometer. For the temperature stabilization of the 8 mm receiver, a Peltier element is used. The noise temperature of the receiver is approximately 280 K. The observational data are recorded in several intensities. Because the measurements are always scaled relative to the quiet-Sun level (QSL), the observations are comparable over the years, and the atmospheric attenuation is not a critical factor when observations are done under good weather conditions. The brightness temperature of the QSL at 8 mm is $8100 \text{ K} \pm 300 \text{ K}$ (Kallunki and Tornikoski, 2018), and the accuracy of identifying the maximum intensity of the faint active regions presented in this study is estimated to be of the order of 0.5 percentage points at the worst. The uncertainty has contributions from the definition of the QSL level, and from the varying sizes of the intensity peaks of active regions.

The solar radio maps are raster scans of 35 sweeps in azimuth direction, and the sweeps are separated by 20 millidegrees. Each of the sweeps consists of 120 data points, so that the distance between samples is ca. 5.8 millidegrees. The final contour map is generated on a rectangular matrix of intensity values through linear interpolation. For each measurement point we have accurate information of the telescope position for defining the coordinates. The time between two consecutive solar radio maps is 172 seconds at the fastest cadence. The full documentation of the RT-14 technical specifications can be found in Kallunki et al. (2012, 2018).

3. Observations

Observations were made in the Summer season 2019 between 1 May and 30 September, a period which includes 153 days in total. The Sun was extremely quiet during that period of time, only a relatively small number of active regions classified by the National Oceanic and Atmospheric Administration (NOAA) (Solar region summary, 2019) were observed. In total, there were 51 days when NOAA classified active regions were identified on the Sun. However, all these active regions were weak, except the active region 12740 which produced some flaring events on 7 May 2019. The maximum intensity of all the radio brightenings from our observing period was from the same active region and it was 112.9% of the QSL intensity. The second highest intensity was (105.9%) observed on 10 May, also from AR 12740.

For our analysis we only wanted to include days without any major activity. The criterion for this is that no formally classified active regions were identified on the solar disk by NOAA on that particular day. The maximum intensity of the radio brightenings during such quiescent days varies between 101% and 103.1% of the QSL (from 8180 K to 8350 K). For comparison, typically the intensity of those radio brightenings that have a connection to a classified active region or sunspot is more than 104%. In addition, 46 days were excluded due to no solar data taken because of the telescope being used for very long baseline interferometry (VLBI) sessions, or because of bad weather conditions.

Thus we were left with 56 days of good-quality radio maps on days of very low activity on the Sun (i.e. with no active regions identified by NOAA). We selected one solar radio map each day close to 12:00 UTC, and all of them were observed between 09:00 and 14:00 UTC, except in three cases. For our analysis we selected the most powerful radio brightening from each map, and in addition to that we identified possible polar radio brightenings. We only selected the most powerful radio brightening in each map to be certain that they represent real features, i.e., to avoid including borderline cases of regions with intensities very close to the QSL intensity.

Table 1 A summary of detected radio brightenings at 8 mm excluding the ones that correlate with coronal holes. The columns list the observing date and time (UT), the maximum intensity of the radio brightening (RB) relatively to the QSL, the latitude (in degrees) of the radio brightening, the longitude (in degrees) of the radio brightening, the atmospheric feature which matches the radio brightening and the source of the loop structure identification. BP = bright point. CL = coronal loop.

Date and time (UT)	Max. inten.	Lat.	Long.	Feature	Loop iden.
01/05/2019 12:02	101.2	33	35	BP	–
27/05/2019 11:55	101.2	–2	51	BP	–
30/05/2019 12:02	101.0	10	24	BP	–
01/06/2019 10:22	102.3	7	–58	BP - CL	EUV 193 Å
02/06/2019 12:53	102.9	5	–45	BP - CL	EUV 193 Å
03/06/2019 12:06	103.1	6	9	BP - CL	EUV 193 Å
07/06/2019 11:40	103.1	5	–26	BP - CL	EUV 193 Å
08/06/2019 11:41	103.1	7	13	BP - CL	EUV 193 Å
09/06/2019 12:12	102.9	9	50	BP - CL	EUV 193 Å
14/06/2019 13:04	101.2	13	56	BP - CL	EUV 211 Å
19/06/2019 11:58	101.0	–22	51	BP	–
23/06/2019 11:35	101.5	–11	52	BP	–
29/06/2019 12:31	102.4	7	–60	BP	–
30/06/2019 12:04	102.6	1	–49	BP	–
01/07/2019 12:42	102.1	3	–33	BP	–
05/07/2019 11:59	102.3	12	40	BP - CL	EUV 211 Å
06/07/2019 12:20	103.0	10	55	BP - CL	EUV 193 Å
27/07/2019 13:31	102.2	13	–28	BP - CL	EUV 211 Å
28/07/2019 12:39	102.1	14	–38	BP - CL	EUV 193/211 Å
29/07/2019 13:18	101.2	7	0	BP - CL	EUV 193/211 Å
30/07/2019 11:57	101.6	10	12	BP - CL	EUV 193/211 Å
31/07/2019 12:00	101.2	6	55	BP	–
01/08/2019 11:59	101.6	8	43	BP	–
02/08/2019 13:01	102.4	10	56	BP	–
03/08/2019 12:11	102.0	3	52	BP - rising fluxes	EUV 211
04/08/2019 11:55	102.4	15	51	BP - rising fluxes	EUV 211
05/08/2019 11:15	102.1	27	56	BP	–
19/08/2019 11:24	101.6	5	53	BP	–
26/08/2019 11:21	101.6	8	55	BP	–
29/08/2019 12:00	101.9	11	53	BP	–
31/08/2019 11:31	101.9	–2	57	BP	–
19/09/2019 05:43	101.8	16	–40	No clear match	–
24/09/2019 10:02	101.0	6	51	Limb activity / No clear match	–
25/09/2019 11:59	102.0	14	51	Limb activity / No clear match	–
26/09/2019 08:03	101.4	17	55	Limb activity / No clear match	–
27/09/2019 10:09	101.7	14	51	BP	–

In Tables 1 and 2 we present a summary of the data. Especially at higher latitudes, the latitude and longitude values are not very accurate due to the low angular resolution of the radio telescope (beamwidth 2.4 arc min). The maximum error is estimated to be 5 degrees at

high latitudes. The majority of the observed features were seen in the northern hemisphere. In Table 2, the radio brightenings which have a connection to coronal hole structures are listed.

4. Results

We compared the location of the maximum radio brightening with data taken at the extreme ultraviolet, EUV. We used the 171, 193 and 211 Å bands for these comparisons. Those bands clearly show coronal bright points and holes, as well as flux structures. Based on our comparison, the observed radio sources reported in this work can in almost all cases be connected to one of the three different atmospheric features: coronal holes or bright points with and without flux tube structure. All observations are listed in Tables 1 and 2.

4.1. Coronal Holes

In Figure 1, a radio map at 8 mm as well as an EUV 193 Å map are presented as an example. The radio brightening and the coronal hole are clearly visible on the north polar region of the solar disk. The red circles indicate the locations of these areas. The maximum radio brightness intensity is 102.6% of the QSL (equivalent to 8310 K).

In total 51 radio brightenings belonging to this category were found. They are listed in Table 2. Overall, the intensity at 8 mm in the direction of the coronal holes varies between 100.7% and 102.6%, with the average being 101.7%, when all radio brightenings belonging to this category are taken into account.

Our limited resolution prevents us from seeing the whole polar region. In addition, we cannot separate small bright features inside the coronal hole structures. In the Summer season of 2019, the northern polar region was better visible for ground-based observatories than the southern one, thus most of the coronal holes which were also seen at 8 mm were located in the north polar regions. In August 2019, we observed an interesting radio brightening which was connected to a coronal hole located near the equator (21 and 22 August).

4.2. Bright Points with Flux Tubes

In Figure 2 we present an example of a radio map at 8 mm and an EUV 171 Å map. The radio source is clearly visible on the left, close to the equator on the solar disk. In the same location, there are several bright points of varying sizes, as well as rising fluxes with open and closed loop structures, which can be seen in the atmospheric imaging assembly (AIA) 171 Å map. In this case, the maximum radio brightness intensity is 102.9% of the QSL (8335 K).

The identified 8 mm regions above bright points with flux tubes are listed in Table 1. Their 8 mm intensities vary between 101.2% and 103.1%, with the average being 102.4%.

4.3. Bright Points Without Flux Tubes

The third case in our analysis are those radio brightenings that match the bright points without rising fluxes. As an example of this category, a radio map at 8 mm and an EUV 193 Å map are presented in Figure 3. We can see a very small bright point in the 193 Å map, which matches the radio brightening. In this case, the intensity of the radio brightening is 101.6% of the QSL (8230 K).

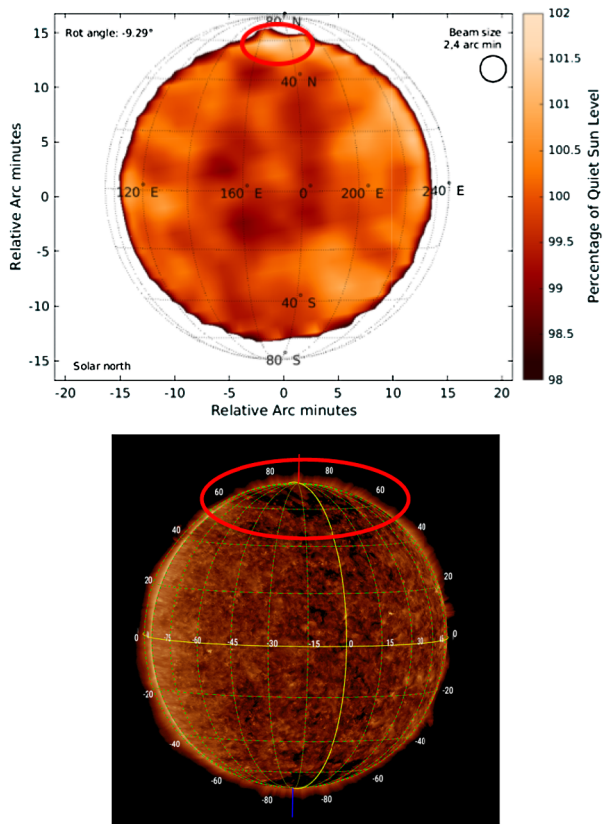
Table 2 A summary of detected radio brightenings at 8 mm that correlate with coronal holes. The columns list the observing date and time (UT), the maximum intensity of the radio brightening (RB) relatively to QSL, the latitude (in degrees) of the radio brightening, the longitude (in degrees) of the radio brightening and the atmospheric feature which matches the radio brightening. CH = coronal hole.

Date and time (UT)	Max. inten. (%)	Lat.	Long.	Feature
01/05/2019 12:02	101.0	50	-11	CH
21/05/2019 12:01	101.5	57	-9	CH
22/05/2019 11:58	101.5	55	-7	CH
01/06/2019 10:22	101.5	56	-3	CH
02/06/2019 12:53	101.8	61	-4	CH
07/06/2019 11:40	101.0	57	-2	CH
08/06/2019 11:41	101.7	60	2	CH
09/06/2019 12:12	101.0	58	-10	CH
14/06/2019 13:04	101.1	57	-17	CH
16/06/2019 12:18	102.0	59	-4	CH
18/06/2019 12:00	101.6	61	8	CH
19/06/2019 11:58	101.0	61	11	CH
23/06/2019 11:35	100.9	58	15	CH
29/06/2019 12:31	101.5	61	2	CH
30/06/2019 12:04	101.4	65	-1	CH
01/07/2019 12:42	100.9	57	-2	CH
05/07/2019 11:59	101.2	63	20	CH
06/07/2019 12:20	101.5	60	-4	CH
19/07/2019 13:15	101.6	61	4	CH
20/07/2019 12:13	101.8	67	13	CH
21/07/2019 13:07	101.7	60	3	CH
28/07/2019 12:39	101.0	63	8	CH
30/07/2019 11:57	101.0	60	3	CH
31/07/2019 12:00	100.8	64	-17	CH
01/08/2019 11:59	101.2	64	-15	CH
02/08/2019 13:01	101.9	63	-9	CH
03/08/2019 12:11	101.5	60	-10	CH
04/08/2019 11:55	101.5	64	-2	CH
05/08/2019 11:15	101.3	64	11	CH
15/08/2019 11:57	101.5	69	2	CH
17/08/2019 12:41	101.5	62	-21	CH
19/08/2019 11:24	101.0	68	1	CH
21/08/2019 11:57	102.0	9	-50	CH (not in polar regions)
21/08/2019 11:57	101.4	67	9	CH
22/08/2019 12:03	102.5	12	-42	CH (not in polar regions)
22/08/2019 12:03	102.0	68	9	CH
24/08/2019 12:22	102.6	63	-4	CH
25/08/2019 11:17	101.2	61	2	CH
26/08/2019 11:21	101.5	63	-6	CH
27/08/2019 11:59	102.0	68	9	CH
28/08/2019 11:56	101.8	67	14	CH

Table 2 (Continued)

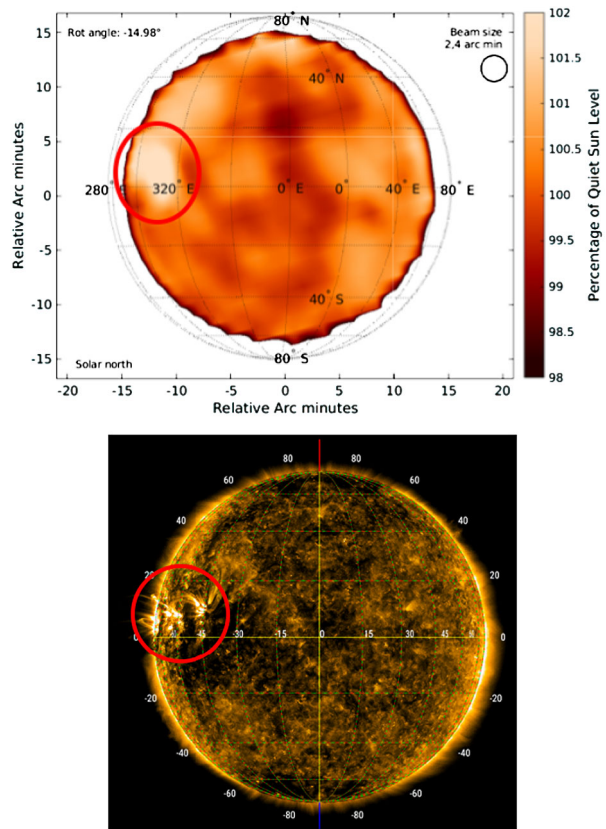
Date and time (UT)	Max. inten. (%)	Lat.	Long.	Feature
29/08/2019 12:00	101.3	64	26	CH
31/08/2019 11:31	100.7	58	31	CH
01/09/2019 12:43	101.5	64	7	CH
17/09/2019 09:19	101.4	63	30	CH
23/09/2019 10:33	101.5	61	6	CH
25/09/2019 11:59	101.4	61	18	CH
26/09/2019 08:03	100.9	65	24	CH
27/09/2019 10:09	101.1	58	38	CH
28/09/2019 10:44	101.7	-3	52	CH (not polar) / No clear match
29/09/2019 10:06	102.1	62	-19	CH / No clear match

Figure 1 In the upper panel, we show an 8 mm solar radio map. In the lower panel, a 193 Å map where a coronal hole is shown. The red circles indicate a coronal hole and a radio brightening. Both maps were observed on 16 June 2019 at 12:17 UT. In the upper panel, the white circle indicates the beam size of the telescope.



The identified 8 mm regions above bright points without flux tube structures are listed in Table 1. Their 8 mm intensities vary between 101.0% and 102.4% of the QSL, with the average being 101.6%. The radio brightenings that belong to this category are weaker than those in the previous category, bright points with flux tubes. Also, their sizes appear to be smaller, even though we did not perform a detailed formal size comparison of all the regions

Figure 2 In the upper panel, we show an 8 mm solar radio map. In the lower panel, we show a 171 \AA map with an active region including rising flux structures. The red circles indicate a bright point and a radio brightening. Both maps were observed on 2 June 2019 at 12:52 UT. In the upper panel, the white circle indicates the beam size of the telescope.



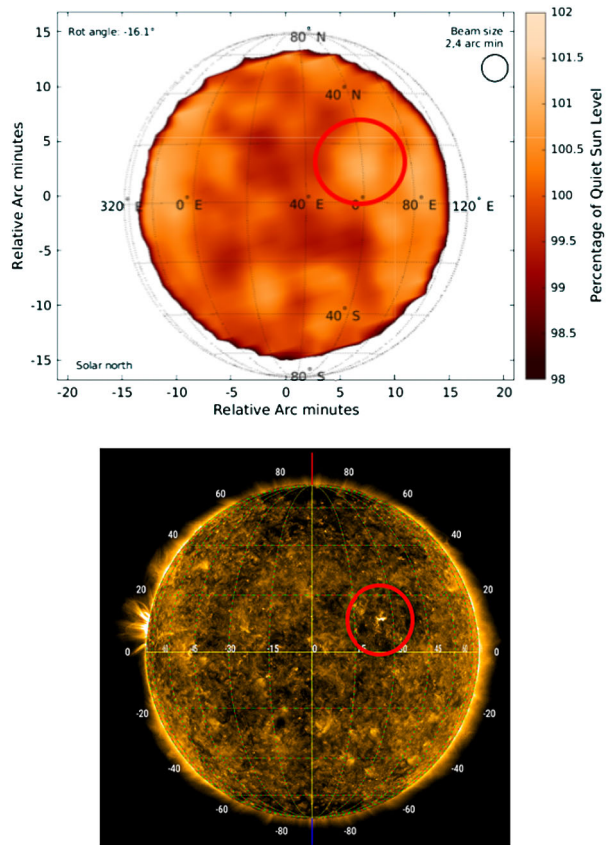
for this study, but only made a robust visual examination of their appearances when initially classifying the radio regions.

5. Conclusion

The strongest radio brightenings during solar minimum are observed in the matching locations where bright points with rising fluxes are seen. The sizes of radio brightenings are also the largest in these areas. For stronger radio brightenings, a formation scenario has been suggested where rising fluxes are observed as a radio source in the higher atmospheric layers; in the case of the 8 mm emission this happens in the chromosphere (Smirnova et al., 2015). No prominent, NOAA class sunspots were observed on these observing days, weaker photospheric features can contribute to the rising magnetic fluxes and the weak radio brightenings reported in this study might be formed in the same way as the stronger radio sources.

The explanation for a radio brightening at the polar regions is analogous to the one above: since there are several open flux structures in the coronal hole, these fluxes push hot plasma into space. The radio source at the polar region can be a result of several features. There are practically always some bright points, such as polar faculae, observed on the Sun. Thus the formation of the radio source could be a contribution from several atmospheric features.

Figure 3 In the upper panel, we show an 8 mm solar radio map. In the lower panel, an 193 \AA map where an active region is shown. The red circles indicate a bright point and a radio brightening. Both maps were observed on 30 May 2019 at 12:02 UT. In the upper panel, the white circle indicates the beam size of the telescope.



Unfortunately our limited resolution of 2.4 arcmin does not enable us to study the detailed structure of the radio brightenings.

The third category, bright points without loop structure, is the most challenging one to explain. Benz et al. (1997) have suggested that the bright points consist of magnetic bipoles, of typically 10^4 km in size, with a mean lifetime of eight hours. This could mean that we have detected those magnetic bipoles as a radio source. We found that, compared to the other two cases presented above, these regions are the weakest. Therefore, we can assume that the rising fluxes are also small and the amount of rising plasma is the smallest in these cases. Possibly these sources are related to solar pores.

In addition to the cases with correlating radio and EUV events discussed above, there was one case where we could not find an atmospheric feature which matches the radio brightening. This event was observed on 19 September 2019, at latitude 5° , longitude 53° , and its maximum intensity was 101.8% of the QSL.

In the future, we plan to carry out a lifetime analysis of all the weak radio brightenings, too. For this article, we studied only one region, and chose the one observed on 3 June 2019. This active region was observed for more than 12 hours and we found that the bright point lived over the whole period. In addition, we found that its intensity varied less than 100 K. To study the intensity profiles of the radio sources in more detail, the observing conditions should be optimal over the whole observing period. Unfortunately, the prevailing weather conditions in the Summer season of 2019 were relatively unstable.

The study that we have reported here shows that some solar activity at millimeter wavelengths is occurring almost all the time, also during the times when solar activity is otherwise very low. For almost all of these radio sources we can find counterparts in the EUV data. This confirms that it is meaningful to continue densely-sampled solar monitoring observations also when no evident major events are recorded, including the transition period from one solar activity cycle into the next one. During the quiescent time it is easier to identify weak active regions that otherwise would go unnoticed, like the polar active regions, and studying their distribution, size, lifetime, intensity profile, and correlation to other wavelength regimes gives us important information about the plasma flows between the solar atmospheric layers.

Acknowledgements This publication makes use of data obtained at the Metsähovi Radio Observatory, operated by the Aalto University. The HMI data are courtesy of NASA/SDO and the AIA, EVE, and HMI science teams. For the EUV images we have used the JHelioviewer, which is part of the open source ESA/NASA Helioviewer Project.

Funding Note Open access funding provided by Aalto University.

Disclosure of Potential Conflicts of Interest The authors declare that there are no conflicts of interest.

Publisher's Note Springer Nature remains neutral with regard to jurisdictional claims in published maps and institutional affiliations.

Open Access This article is licensed under a Creative Commons Attribution 4.0 International License, which permits use, sharing, adaptation, distribution and reproduction in any medium or format, as long as you give appropriate credit to the original author(s) and the source, provide a link to the Creative Commons licence, and indicate if changes were made. The images or other third party material in this article are included in the article's Creative Commons licence, unless indicated otherwise in a credit line to the material. If material is not included in the article's Creative Commons licence and your intended use is not permitted by statutory regulation or exceeds the permitted use, you will need to obtain permission directly from the copyright holder. To view a copy of this licence, visit <http://creativecommons.org/licenses/by/4.0/>.

References

- Alissandrakis, C.E., Patsourakos, S., Nindos, A., Bastian, T.S.: 2017, *Astron. Astrophys.* **605**, A78. DOI.
- Benz, A.O., Krucker, S., Acton, L.W., Bastian, T.S.: 1997, *Astron. Astrophys.* **320**, 993.
- Bogod, V.M., Stupishin, A.G., Yasnov, L.V.: 2012, *Solar Phys.* **276**, 61. DOI.
- Cho, I.-H., Cho, K.-S., Bong, S.-C., Lim, E.-K., Kim, R.-S., Choi, S., Kim, Y.-H., Yurchyshyn, V.: 2015, *Astrophys. J.* **811**, 49. DOI.
- Doschek, G.A., Warren, H.P., Laming, J.M., Mariska, J.T., Wilhelm, K., Lemaire, P., Schühle, U., Moran, T.G.: 1997, *Astrophys. J.* **482**, L109. DOI.
- Giordano, S., Berrilli, F., Del Moro, D., Penza, V.: 2008, *Astron. Astrophys.* **489**, 747. DOI.
- Kallunki, J., Tornikoski, M.: 2018, *Solar Phys.* **293**, 156. DOI.
- Kallunki, J., Uunila, M.: 2017, *Astron. Nachr.* **338**, 398. DOI.
- Kallunki, J., Lavonen, N., Järvelä, E., Uunila, M.: 2012, *Balt. Astron.* **21**, 255. DOI.
- Kallunki, J., Tornikoski, M., Tammi, J., Kinnunen, E., Korhonen, K., Kesäläinen, S., Arkko, O.: 2018, *Astron. Nachr.* **339**, 204. DOI.
- Nitta, N.V., Sun, X., Hoeksema, J.T., DeRosa, M.L.: 2014, *Astrophys. J.* **780**, L23. DOI.
- NOAA Space Weather Prediction Center - Daily solar region summary, 2019. <https://www.swpc.noaa.gov/products/solar-region-summary>.
- Oliveira e Silva, A.J., Selhorst, C.L., Simões, P.J.A., Giménez de Castro, C.G.: 2016, *Astron. Astrophys.* **592**, A91. DOI.
- Pohjolainen, S.: 2000, *Astron. Astrophys.* **361**, 349.
- Pohjolainen, S., Riehkainen, A., Valtaoja, E.: 1999, In: *Magnetic Fields and Solar Processes*, 635.
- Riehkainen, A., Urpo, S., Valtaoja, E., Makarov, V.I., Makarova, L.V., Tlatov, A.G.: 2001, *Astron. Astrophys.* **366**, 676. DOI.

- Rodger, A.S., Labrosse, N., Wedemeyer, S., Szydlarski, M., Simões, P.J.A., Fletcher, L.: 2019, *Astrophys. J.* **875**, 163. [DOI](#).
- Selhorst, C.L., Giménez de Castro, C.G., Valio, A., Costa, J.E.R., Shibasaki, K.: 2011, *Astrophys. J.* **734**, 64. [DOI](#).
- Selhorst, C.L., Simões, P.J.A., Oliveira e Silva, A.J., Giménez de Castro, C.G., Costa, J.E.R., Valio, A.: 2017, *Astrophys. J.* **851**, 146. [DOI](#).
- Smirnova, V.V., Solov'ev, A.A., Riehoainen, A., Kallunki, J.: 2015, *Geomagn. Aeron.* **55**, 991. [DOI](#).
- Sudar, D., Brajša, R., Skokić, I., Benz, A.O.: 2019, *Solar Phys.* **294**, 163. [DOI](#).
- Sütterlin, P., Schröter, E.H., Muglach, K.: 1996, *Solar Phys.* **164**, 311. [DOI](#).